NMR spectroscopy of the normal and superconducting states of MgB₂ and comparison to AlB₂

S. H. Baek,[1] B. J. Suh,[2] E. Pavarini,[3] F. Borsa,[1,3] R. G. Barnes,[1] S. L. Bud'ko,[1] and P. C. Canfield[1]

[1]*Department of Physics and Astronomy and Ames Laboratory, Iowa State University, Ames, Iowa 50011*
[2]*Department of Physics, the Catholic University of Korea, Puchon, 420-743, Korea*
[3]*Department of Physics "A. Volta" and Unita' INFM di Pavia, Via Bassi 6, I27100 Pavia, Italy*

^{11}B NMR measurements have been performed in [11]B enriched MgB₂ powder samples in external fields of 0.813, 1.55, 4.7, and 7.2 T both in the normal phase and in the superconducting phase. A previously unreported dipolar Pake doublet has been observed in the quadrupole perturbed NMR spectrum. The Knight shift can thus be accurately determined by narrowing the line with the magic angle spinning (MAS) technique. Results of Knight shift (K) and relaxation rates ($1/T_1$) for both [11]B and [27]Al nuclei are reported also for AlB₂. The comparison of the data in the two compounds shows the dramatic drop of the density of states at the boron site in AlB₂ with respect to MgB₂. The experimental values for K and $1/T_1$ are in most cases in good agreement with the theoretical values obtained from first principles calculations. The recovery of the nuclear magnetization below T_c in random powder samples is nonexponential due to the anisotropy of the upper critical field. The exponential drop of $1/T_1$ in the superconducting phase observed by Kotegawa *et al.* is confirmed here but not the coherence peak.

I. INTRODUCTION

After the discovery of superconductivity[1] in MgB₂ with $T_c \sim 39$ K and subsequent observation of boron isotope effect[2,3] confirming that MgB₂ is a phonon-mediated BCS superconductor, much effort have been devoted to this intermetallic compound up to date due to its remarkably high-T_c among BCS superconductors.

Nuclear magnetic resonance (NMR) is a suitable microscopic tool to investigate the electronic structure in the normal state, the structure of the gap and the flux line lattice in the superconducting state.[4] This justifies the large number of studies by both ^{11}B and [25]Mg NMR in MgB₂ which have already appeared in the literature.[5–11]

Regarding the ^{11}B NMR, there is substantial agreement about the measurements of the quadrupole coupling constant ν_Q and about the nuclear spin-lattice relaxation rate $1/T_1$ in the normal phase. On the other hand, there is considerable controversy concerning the [11]B Knight shifts in the normal phase and about the temperature dependence of $1/T_1$ in the superconducting phase. In the present paper, we report new results for the ^{11}B NMR spectrum in the normal phase and an accurate determination of the Knight shift by using the magic angle spinning (MAS) technique. We also find an explanation for the discrepancies in the results of $1/T_1$ below T_c reported by different authors, based on the strong anisotropy of the upper critical field in MgB₂.

Since NMR in metals probes the density of states (DOS) at the Fermi level, we have performed measurements of both ^{11}B and ^{27}Al NMR in AlB₂ in order to compare the DOS in the two compounds. Finally the experimental results for Knight shifts and relaxation rates in both MgB₂ and AlB₂ have been compared with *ab initio* calculations.

II. EXPERIMENTAL DETAILS AND SAMPLE PREPARATION

MgB₂ crystallizes in the hexagonal AlB₂ type structure, which consists of alternating hexagonal layers of Mg atoms and graphitelike honeycomb layers of B atoms. Powder samples were prepared with the method described in Ref. 2. X-ray powder diffraction measurements confirmed the hexagonal unit cell of MgB₂.[1,2] Magnetization measurements done at $H = 2.5$ mT yield a transition temperature $T_c = 39.2$ K with a shielding volume fraction close to 100%.[2,12,13] We have investigated several samples from different batches of polycrystalline [11]B enriched MgB₂ in order to check the reproducibility of the data. The samples enriched (about 99%) in [11]B were the same used for the observation of the isotope effect.[2] Although for NMR one could use the natural abundance samples we found that the use of [11]B enriched samples has helped to resolve the dipolar splitting and thus to make the measurements less ambiguous. Also we have performed measurements in samples from the same batch both in bulk and in powder ground to different particle size. No substantial differences were observed in the NMR measurements in the different samples. The onset of superconductivity was also determined by monitoring the detuning of the NMR circuit occurring at the irreversibility temperature T_{irr}. This type of measurement corresponds to probing the temperature dependence of the radio frequency (rf) surface resistance.[5] Thus, as the magnetic field is increased the transition region broadens due to the dissipation associated with flux line motion below T_c, and at 7.2 T no detuning can be observed although the magnetization measurements indicate a $T_c = 23$ K at 7 T.[5] The transition temperature at 4.7 T was found to be $T_c = 27.5$ K and at 1.55 T, $T_c = 34$ K.

^{11}B and ^{27}Al NMR and spin-relaxation measurements were performed with home built Fourier transform (FT) pulse spectrometers operating at variable frequencies. The $\pi/2$ radio frequency (rf) pulse length was typically 6 μs. The magic angle spinning (MAS) experiment was performed with a home built spinning probe with a maximum spinning frequency of about 10 kHz.

III. ^{11}B NMR IN MgB$_2$ IN THE NORMAL STATE

The ^{11}B NMR spectrum in MgB$_2$ powder samples is complicated by the simultaneous presence of first and second order quadrupole interactions, anisotropic Knight shift, and a previously unnoticed dipolar splitting which is particularly evident in ^{11}B isotopically enriched samples. In the following we analyze the different spectral features, a necessary step in order to extract reliable NMR parameters.

A. Quadrupole interactions

The complete ^{11}B NMR spectrum was published before.[5] For spin $I = 3/2$, with electric quadrupole moment Q and for an axially symmetric electric field gradient tensor (EFG) with maximum component q the separation of the two symmetric satellite lines is[14]

$$\Delta \nu = \nu_Q (3 \cos^2 \theta - 1) \quad \text{with} \quad \nu_Q = \frac{e^2 qQ}{2h}, \quad (1)$$

where θ is the angle between the principal axis of the EFG tensor and the applied field H_0.

From the frequency separation of the satellites lines a temperature independent $\nu_Q = 835 \pm 10$ kHz was found.[5] A small increase in the quadrupole coupling constant with decreasing temperature was observed in ^{111}Cd perturbed angular $\gamma\gamma$ correlation (TDPAC) experiments[6] and is consistent with the effect of lattice vibrations.[15]

In the presence of second order quadrupole effects the central line transition is shifted. For axially symmetric EFG this results in a powder pattern with two singularities separated by

$$\delta \nu = \frac{25}{48} \frac{\nu_Q^2}{\nu_L}, \quad (2)$$

where ν_L is the nuclear Larmor frequency. Because of the inverse Larmor frequency dependence in Eq. (2) the two singularities can be resolved only at low magnetic field as shown in Fig. 1(a). At lower fields (1.55 and 0.813 T), the second order quadrupole splitting is well resolved and each singularity is split into a doublet. If one takes the middle point of each doublet, the distance between singularities is in good agreement with that calculated from Eq. (2) and the value of ν_Q determined from the separation of the satellite lines, i.e., $\delta\nu = 32.7$ kHz at 0.813 T [see Fig. 1(b)]. One unexpected feature is that the two singularities are each split into a field independent doublet. At higher fields (4.7 and 7.2 T), the second order quadrupole splitting is negligible and only one doublet is shown.

B. Dipolar doublet

As shown in Fig. 1(a) at high fields, where the second order quadrupole effects become negligible, the ^{11}B NMR spectrum is formed by a doublet. At low fields one can clearly resolve two doublets, one for each singularity in the quadrupole powder pattern. The splitting is temperature and field independent and results from the nearest neighbor nuclear dipolar interaction of ^{11}B nuclei in the planar hon-
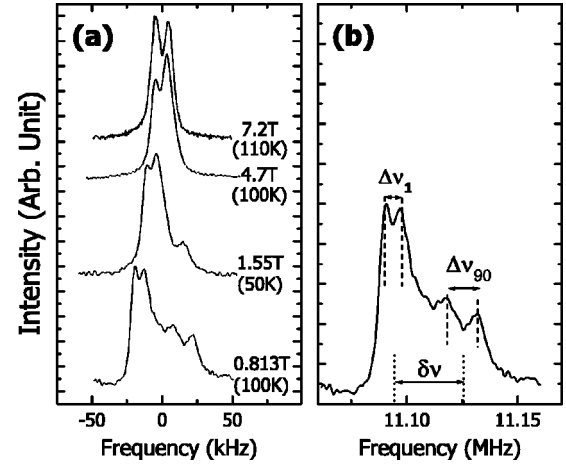
FIG. 1. (a) Central line transition of ^{11}B NMR spectrum for powder sample of MgB$_2$ at several representative magnetic fields. (b) Spectrum at 0.813 T. The distance between the middle point of each doublet corresponds to the second order quadrupole splitting $\delta\nu$.

eycomb lattice structure. In such a structure each ^{11}B nucleus is strongly coupled to three nearest neighbors resulting in three equivalent doublets which bear resemblance with the well known Pake doublets.[16] A single dipolar pair gives rise to a Pake doublet in the NMR spectrum with frequencies

$$\nu_{\pm} = \nu_L \pm \nu_D (3 \cos^2 \theta' - 1) \quad (3)$$

with

$$\nu_D = \frac{3}{2} \frac{\gamma\mu}{2\pi a^3}, \quad (4)$$

where θ' is the angle formed by the magnetic field with the vector joining the two interacting nuclei, μ is the nuclear magnetic moment, and a is the internuclear distance.

In the presence of three interacting pairs one has to sum over the different angles and take the powder average including the second order quadrupole interaction and the anisotropic Knight shift interaction. The situation was analyzed previously in connection with measurements in intermetallic compounds of the C32 (AlB$_2$) structure.[17] The conclusion was reached that in the C32 structure the resonance line in the presence of all the above interactions can be described in terms of the angle θ formed by the magnetic field and the c axial symmetry axis perpendicular to the B plane. Thus it was predicted that the $\theta = 90°$ singularity in the quadrupole pattern should be split into two lines separated by $\Delta\nu_{90} = 3\nu_D$ while the intermediate angle singularity should be split into two lines separated by $\Delta\nu_1 = 2\nu_D$. From the inspection of Fig. 1(b) one can see that the ratio of the two splittings is in reasonable agreement with the above prediction. Furthermore, by using in Eq. (4) $\gamma = 13.66 \times 2\pi$ MHz/T, $\mu = I\gamma h/2\pi$ and the measured value $\nu_D = 4.00 \pm 0.50$ kHz (at 0.813 T), one obtains the B-B nearest neighbor distance $a = 1.72 \pm 0.08$ Å in agreement with the known value of 1.782 Å.
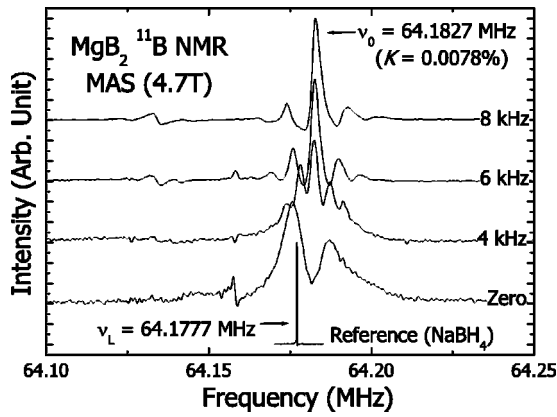
FIG. 2. Magic angle spinning (MAS) experiment in MgB_2 powder sample at 4.7 T. Spinning frequencies are shown at the right side of the figure.

C. Knight shift

In order to determine the Knight shift, both isotropic and anisotropic parts, measurements should be made at very high magnetic fields ($H \gg 10$ T) where the second order quadrupole effects are negligible, and the anisotropic Knight shift may be inferred from the asymmetric broadening of the NMR line.[17] Since our measurements are limited to a maximum field of 7.2 T no measurable anisotropic Knight shift could be detected. The isotropic Knight shift K is measurable but very small. Its measurement is further complicated by the dipolar splitting discussed above. In order to obtain a reliable value of K we performed a magic angle spinning (MAS) experiment[18] at room temperature in a field of 4.7 T. As shown in Fig. 2, the dipolar splitting is totally removed for a spinning frequency of 8 kHz as well as part of the dipolar broadening and of the quadrupole broadening. From the resulting narrow line we obtain $K = 80$ ppm with respect to a reference solution of $NaBH_4$. If the Knight shift is referred to the BF_3 solution, which is the compound used by chemists as the "zero chemical shift,"[19] one obtains $K = 40 \pm 10$ ppm.

D. Nuclear spin-lattice relaxation rate

For the case of saturation of the central line of the ^{11}B NMR spectrum with a single rf pulse (or short sequence of pulses) and for magnetic relaxation mechanism, the recovery of the nuclear magnetization after a time t following saturation is given by[20]

$$\frac{M(\infty) - M(t)}{M(\infty)} = 0.1 \exp(-2Wt) + 0.9 \exp(-12Wt), \quad (5)$$

where we define the nuclear spin lattice relaxation rate as $1/T_1 = 2W$. The results for the temperature dependence of $1/T_1$ are shown in Fig. 3. As can be seen, a field independent linear temperature dependence is observed in the normal phase yielding $T_1T = 170$ sK.
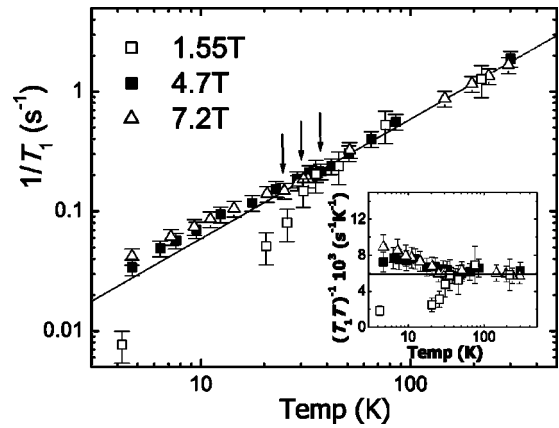
FIG. 3. Temperature dependence of $1/T_1$ for ^{11}B in MgB_2 at external fields 1.55, 4.7, and 7.2 T. The line is the Korringa law with $T_1T = 170$ sK. The three arrows indicate the superconducting transition temperatures at each field which are 23, 27.5, and 34 K, respectively. In the inset, $(T_1T)^{-1} \times 10^3$ is plotted against temperature.

IV. ^{11}B AND ^{27}Al NMR IN AlB_2

The room temperature ^{11}B NMR spectrum on the powder sample of AlB_2 is very similar to the one for MgB_2.[5] From the separation of the satellite lines one derives a quadrupole coupling frequency $\nu_Q = 540 \pm 10$ kHz somewhat smaller than the one in MgB_2. The central transition linewidth at room temperature is about 19 kHz and it hides the dipolar splitting discussed for the case of MgB_2 due to the stronger dipolar interaction with the ^{27}Al nuclei present in AlB_2. By spinning the sample at 10 kHz we obtain a MAS NMR line 2 kHz wide. The Knight shift value with respect to a reference solution of BF_3 measured from the MAS spectrum is found to be $K = -10 \pm 5$ ppm. Finally, the $1/T_1$ measurements as a function of temperature shown in Fig. 4 yield a Korringa law with $T_1T = 1400$ sK, i.e., almost one order of magnitude greater than in MgB_2.

The room temperature ^{27}Al ($I = 5/2$) NMR spectrum in AlB_2 is composed of a central transition line 23 kHz wide
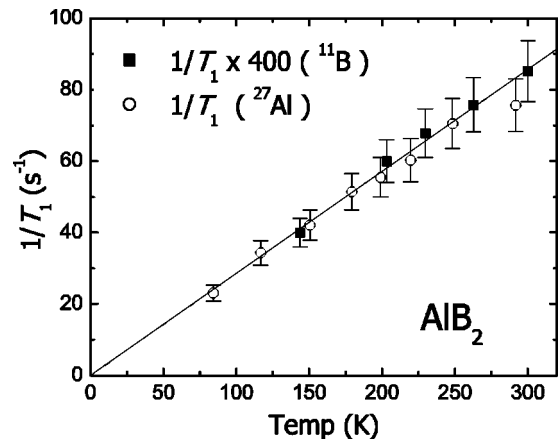
FIG. 4. Comparison of $1/T_1$ for ^{11}B and for ^{27}Al in AlB_2 powder sample. T_1T for ^{27}Al is 400 times smaller than the value for ^{11}B.

TABLE I. Summary of the various experimental NMR parameters for both MgB_2 and AlB_2. The Korringa ratio R is defined as $R = K^2 T_1 T/S$. Results for ^{25}Mg NMR were taken from Ref. 7.

| | MgB_2 | | AlB_2 | |
	^{25}Mg (Ref. 7)	^{11}B	^{27}Al	^{11}B
K (ppm)	242 ± 4^a	$+40 \pm 10^b$	$+880 \pm 20^c$	-10 ± 5^b
$T_1 T$ (sK)	1090	170	3.5	1400
S (sK)	7.03×10^{-5}	2.57×10^{-6}	3.88×10^{-6}	2.57×10^{-6}
R	0.95	0.102 ± 0.05	0.7 ± 0.03	$0 - 0.12$
ν_Q (kHz)	222 (1.5)	835 (10)	80 (10)	540 (10)

^{a}Reference solution $MgCl_2$.
^{b}Reference solution BF_3.
^{c}Reference solution $AlCl_3$.

and a poorly-resolved powder pattern originating from the two satellite pairs over a spectral distribution of about 200 kHz. From the fit of the NMR spectrum to a computer simulated spectrum with a Gaussian dipolar width of 7.5 kHz one can derive a quadrupole coupling constant $\nu_Q = 80 \pm 10$ kHz. It is assumed that the electric field gradient has axial symmetry as for the ^{11}B site. The Knight shift was measured from the position of the central line transition (which has a negligible second order quadrupole broadening). The Knight shift with respect to a $AlCl_3$ aqueous solution is $K = 880 \pm 20$ ppm.

The ^{27}Al $1/T_1$ results as a function of temperature are shown in Fig. 4 together with the ^{11}B results. The linear temperature dependence yields for ^{27}Al $T_1 T = 3.5$ sK which is 400 times smaller than the value for ^{11}B.

The various NMR parameters for both MgB_2 and AlB_2 are summarized in Table I. The constant S listed in Table I is given by $S = (\gamma_e/\gamma_n)^2 h/(8\pi^2 k_B)$ and the Korringa ratio R is defined as $R = K^2 T_1 T/S$.

V. COMPARISON OF THEORY AND EXPERIMENTS IN MgB_2 AND AlB_2

In order to understand the microscopic origin of the relaxation, and thus also the differences between AlB_2 and MgB_2, a comparison between experimental and *ab initio* calculated values of Knight shifts and relaxation rates is highly desirable. Recently, first principles calculation of the relaxation rates[21,22] and the Knight shifts[21] were performed for MgB_2. In Ref. 22 the relaxation rates were calculated for AlB_2 as well. In the present work we calculate K and $1/T_1 T$ for AlB_2 by using the method described in Ref. 21, and compare the results for MgB_2 and AlB_2. Our calculations are based on density functional theory (DFT) in the local density approximation (LDA). We adopt the tight binding linear-muffin-tin-orbital (LMTO) method[23] in the atomic-spheres approximation (LMTO47 Stuttgart code). The density of states matrix [Eq. (2) of Ref. 21] and the partial density of states N_L (with $L = lm$, where l is the orbital angular momentum quantum number, and $m = -l, \ldots, l$) were calculated by using the linear tetrahedron method. We found that the results already converged very well with a mesh of 481 irreducible **k** points. In order to obtain accurate wave functions at the Fermi level,

TABLE II. Calculated Knight shifts in ppm and $1/T_1 T$ in 10^{-3}/sK in AlB_2. The label $\alpha = x,y,z$ indicates the direction of the external magnetic field.

K	dipole (xy)	dipole (z)	orbital	Fermi contact	core
B	-8	16	0	61	-11
Al	1	-2	0	660	-15
$1/T_1 T$	dipole	orbital	Fermi contact	core	
B	0.086	0.132	1.4	0.04	
Al	0.115	0.370	105	0.05	

the linear partial wave expansion was performed with $\epsilon_\nu \equiv \epsilon_F$, where ϵ_F is the Fermi level and ϵ_ν the expansion energy. Further details about the method employed can be found in Ref. 21.

In Table II, we show the calculated contributions to K and $1/T_1 T$ for AlB_2. The corresponding quantities for MgB_2 are reported in Table I and II of Ref. 21.

Let us discuss first the case of MgB_2. The ^{11}B orbital relaxation rate is about 3 times larger than the dipolar, and about 10 times larger than the Fermi-contact term. As explained in Ref. 21, the reason is the following. In MgB_2 the B p_σ and B p_π bands are all at the Fermi level: the partial density of states $N_{p_{x,y}}$ (σ bands) and N_{p_z} (π bands) are, respectively, $N_{p_x} = N_{p_y} \sim 0.035$ states/eV/spin/B, and $N_{p_z} \sim 0.045$ states/eV/spin/B. On the contrary, there are very few B s electrons close to ϵ_F ($N_s \sim 0.002$ states/eV/B). An approximate formula for the ratio between the Fermi contact and the orbital/dipolar coupling constants is given by[21]

$$F = \frac{2}{3} \frac{|\phi_s(0)|^2 N_s}{\sum_{l>0} \langle r^{-3} \rangle_{ll} N_l}. \tag{6}$$

Here $\phi_l(r)$ is the l radial solutions of the Schrödinger equation at energy ϵ_ν and $N_l \equiv \Sigma_{m=-l}^{m=l} N_{lm}$. In addition $\langle r^{-3} \rangle_{ll} \equiv \int [|\phi_l(r)|^2/r^{-3}] r^2 dr$ and $\phi_s(0) \equiv \phi_{l=0}(r=0)$, where $r = 0$ is the position of the nucleus. In the case of B it was found[21] $F \sim 0.35$. Thus F is considerably smaller than 1, and the Fermi contact interaction (which usually dominates over the orbital and dipolar mechanisms) gives only a small contribution to the relaxation rate. Moreover, since $N_{p_x} = N_{p_y} \sim N_{p_z}$, one can show analytically[21] that the ratio between orbital/dipolar relaxation rate is about 3.3.

The case of ^{25}Mg is different: $F \sim 5 \gg 1$, and thus the Fermi contact interaction dominates. With a Stoner enhancement factor of about 1.33 (calculated *ab initio* in Ref. 21), the following results were found for the total Knight shifts $K(Mg)(xy/z) \sim 361/341$ ppm and $K(B) \sim 24/42$ ppm. For the relaxation time, it was shown[21] that the Stoner enhancement factor is about 1.6. Thus the total relaxation times are: $T_1 T(Mg) \sim 625$ sK and $T_1 T(B) \sim 169$ sK. These results are in quite good agreement with experimental data as evinced from the comparison of Tables III and I.

Let us now discuss the case of AlB_2. In this compound the B p_σ bands are fully occupied, and only B p_π bands are

TABLE III. Summary of the total calculated relaxation rates and Knight shifts (without Stoner factor) in MgB_2 and AlB_2 to be compared with the experimental results in Table I. The values for MgB_2 are taken from Ref. 21.

	MgB_2		AlB_2	
	^{25}Mg	^{11}B	^{27}Al	^{11}B
K (xy/z) in ppm	271/256	16/28	644/647	42/66
T_1T in sK	1000	270	9	603

at the Fermi level. In addition $|\phi_s(0)|^2/4\pi \sim 2.87\,a_0^3$ and $N_s \sim 0.003$ states/eV/spin/B, $\langle r^{-3}\rangle_{11} \sim 1.45\,a_0^3$ and $N_p \sim 0.0216$ states/eV/spin/B. With these numbers we find $F \sim 2.3$; terms with $l>1$ give a small contribution to F, because the radial integrals decrease quickly when l increases and because, in the case of B, N_l is very small for $l>1$. Thus F is considerably larger than 1, and the Fermi contact interaction is the dominant mechanism of relaxation for ^{11}B (see Table II). The same happens for ^{27}Al, for which we find $|\phi_s(0)|^2/4\pi \sim 2.96\,a_0^3$ and $N_s \sim 0.0362$ states/eV/spin, $\langle r^{-3}\rangle_{11} \sim 1.74\,a_0^3$ and $N_p \sim 0.0325$ states/eV/spin/B, and therefore $F \sim 16$.

In order to understand better the numerical results for AlB_2, we calculate analytically the contact shift and relaxation rates for a model Hamiltonian which includes only B s and Al s states. Within this model, the Knight shift is given by $K \sim \mu_B^2(4/3)|\phi_s(0)|^2 N_s$, and the relaxation rate can be obtained from the Korringa relation. We find $K(Al) \sim 645$ ppm, $K(B) \sim 52$ ppm and $1/T_1T(Al) \sim 107 \times 10^{-3}/(sK)$, $1/T_1T(B) \sim 1.05 \times 10^{-3}/(sK)$, in very good agreement with the first principles values (see Table II).

The *ab initio* total Knight shifts (Table III) are $K(Al) \sim 644/647$ ppm and $K(B) \sim 42/66$, and the total relaxation times (Table III) are $T_1T(Al) \sim 9$ sK and $T_1T(B) \sim 603$ sK. The agreement between first principle results and experimental data is quite good for Al. In the case of B the calculated relaxation time is about 2 times smaller than the experimental data. Similar[24] results were found in Ref. 22. This discrepancy could suggest that, in the case of AlB_2, LDA tends to slightly overestimate the Fermi-contact interaction at the B nucleus. Furthermore the calculated Knight shift is in total disagreement with the experimental result and the Korringa ratio is anomalously low. These inconsistencies are most likely related to the very small K value which makes the experimental result quoted extremely sensitive to the "zero chemical shift" reference used.

Finally, we point out that in AlB_2 the density of states in the B plane is strongly reduced with respect to MgB_2. The reason is that in AlB_2 the σ bands are well below ϵ_F, while in MgB_2 they cross the Fermi level. We find $N_{p_x}+N_{p_y} \sim 0.0046$ and $N_{p_z} \sim 0.017$ states/eV/spin/B, while for MgB_2 $N_{p_x}+N_{p_y} \sim 0.07$ and $N_{p_z} \sim 0.045$ states/eV/spin/B was found.[21]

VI. ^{11}B NMR IN MgB_2 IN THE SUPERCONDUCTING PHASE

Although the main emphasis of the present paper is on the electronic properties of MgB_2 in the normal phase, it is
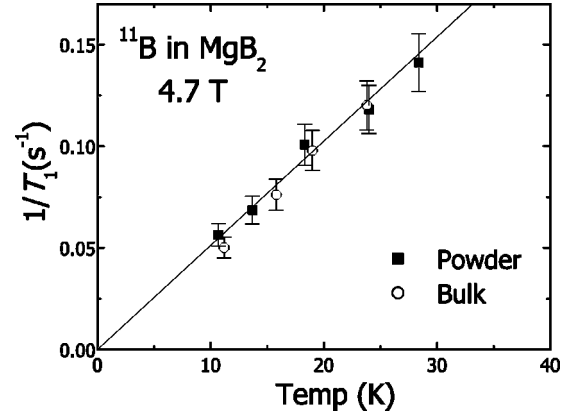
FIG. 5. $1/T_1$ results for ^{11}B in a powder and in a sintered bulk sample of MgB_2 below T_c.

worthwhile to present and discuss here the ^{11}B NMR results obtained in the superconducting phase mostly to point out the limitations incurred in the NMR experiments in polycrystalline samples.

Regarding the Knight shift, one can conclude that no meaningful measurements of K can be performed below T_c in a powder sample. In fact the Knight shift is very small compared to the line broadening due to the magnetic field distribution of the flux line lattice.[8] Furthermore the correction for the shift due to the diamagnetic shielding in the superconducting phase cannot be estimated accurately in a powder sample as a result of the distribution of shapes of the particles e.g. distribution of demagnetization factors.

The temperature dependence of $1/T_1$ below T_c allows in principle to obtain information about the pairing symmetry and the structure of the superconducting gap.[25,26] In fact the ratio of the relaxation rates in the superconducting phase and the normal phase $(1/T_{1s})/(1/T_{1n})$ is related to the density of states in the superconducting phase and should decrease below T_c either exponentially or with a power law depending on the pairing symmetry and/or the structure of the gap.[9] As can be seen in Fig. 3 a decrease of the relaxation rate below T_c can be observed in the data taken in an external field of 1.55 T but not in the data at 4.7 and 7.2 T. The explanation for this is easily found in the strong anisotropy of the upper critical field H_{c2}. The powders utilized in the present experiment have $H_{c2}^{max}/H_{c2}^{min}=\gamma \approx 6$ whereby the maximum critical field pertains to the particles with the field in the ab plane.[27,28] In a detuning experiment one detects the superconducting transition of the particles which have the higher upper critical field (see arrows in Fig. 3). On the other hand in the NMR experiment the stronger signal arises from the particles which are oriented in such a way as to have the lower upper critical field. This is a consequence of the strongly reduced rf penetration length and consequently reduced NMR signal, in the superconducting particles. Thus the results in Fig. 3 for fields of 4.7 and 7.2 T pertain mostly to the particles which remain in the normal phase down to helium temperature. It should be noted that the results in a loose powder and in a polycrystalline bulk (sintered) sample are the same as shown in Fig. 5.
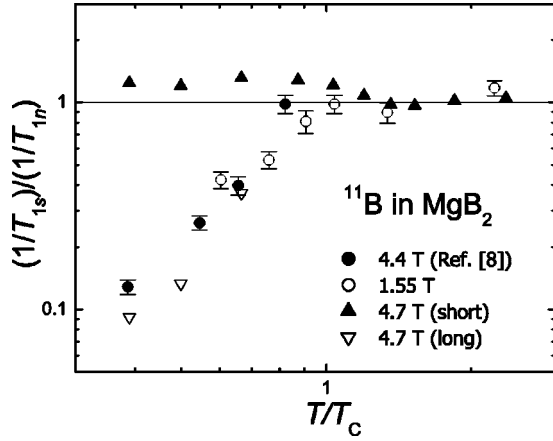
FIG. 6. The plot of the ratio of $1/T_1$ in the superconducting phase and the normal phase against T/T_c. The short and long components of the relaxation rate at 4.7 T were obtained by fitting the data to Eq. (5) with two different values of W.

Our results need to be reconciled with the ^{11}B NMR data in MgB$_2$ by Kotegawa *et al.*[9] where it is reported that $1/T_1$ decreases exponentially below T_c in powder samples for all field values from 1.35 up to 4.42 T with a tiny coherence peak just below T_c. First it is noted that the samples used in Kotegawa's experiments could have a much smaller anisotropy of the upper critical field. Recent resistivity measurements in MgB$_2$ single crystals yield an anisotropy ratio of the upper critical field of only 2.7.[29] A second factor is that our measurements were done by fitting the first 90% of the recovery of the nuclear magnetization which yields the short component only of the relaxation. On the other hand the results reported by Kotegawa *et al.* were obtained by fitting the recovery of the magnetization with two components and assuming that the long component only is the one pertaining to the superconducting particles.[30] By following the same procedure i.e. by fitting the recovery of the nuclear magnetization with Eq. (5) with two different values of W we find the results shown in Fig. 6. The long component does indeed agree with Kotegawa's data at high field (4.7 T) and with our low field data (1.55 T) although it appears doubtful that the data below T_c can be sufficiently precise to differentiate between single gap and two-gap behavior.[31] In fact the distribution of critical fields due to the random orientation of the particles in a powder sample introduces large errors in the evaluation of $1/T_1$ particularly close to T_c since the recovery of the magnetization is the superposition of curves, Eq. (5), with different W values. In particular it is very difficult to infer the presence of a coherence peak in $1/T_1$ just below T_c as claimed by Kotegawa *et al.*[9] It is noted that from the data in the inset of Figs. 3 and 6 there appears to be a enhancement of $(T_1T)^{-1}$ over the Korringa value of the normal phase starting at T_c and extending to low temperature. This effect, which is barely outside the experimental error, is not presently understood. One may speculate that the measured $1/T_1$ in Fig. 3 is an average of the relaxation of nuclei in particles in the normal phase and particles in the superconducting phase with H perpendicular to the ab plane in which the relaxation is enhanced by the

presence of flux lines.[4] More detailed measurements as a function of magnetic field are needed to elucidate this point.

VII. SUMMARY AND CONCLUSIONS

From the analysis of the ^{11}B NMR spectrum in the normal phase of isotopically enriched MgB$_2$, we have found evidence for a field independent splitting of the line due to the nuclear dipolar interaction (Pake doublet). By averaging out the dipolar interaction with magic angle spinning, we have obtained reliable values for the Knight shifts for ^{11}B in both MgB$_2$ and AlB$_2$. Both the decrease of K and more so of $(T_1T)^{-1}$ for ^{11}B in AlB$_2$ with respect to MgB$_2$ is in qualitative agreement with a drastic drop of the DOS at the Fermi level at the B site in AlB$_2$. The *ab-initio* calculated values for ^{11}B (see Table III) are in excellent agreement with the experimental ones in MgB$_2$ provided the theoretical Knight shift is multiplied by a Stoner enhancement factor of 1.33 and the theoretical $1/T_1T$ by a Stoner factor of 1.6. The agreement in MgB$_2$ is slightly less good for then ^{25}Mg nucleus if the same Stoner factors are used.

For the case of AlB$_2$ the *ab initio* calculated values are in good agreement with the experiments only for the ^{27}Al data considering that the theoretical results in Table III are still to be multiplied by the Stoner factor. However, for the B site in AlB$_2$ the theoretical values for both K and $(T_1T)^{-1}$ are bigger than the experimental values indicating that the LDA calculations overestimate the Fermi contact interaction at the B nuclear site.

Regarding the superconducting phase in MgB$_2$, we conclude that it is very difficult to obtain reliable information for the NMR parameters (particularly the relaxation rates) from polycrystalline samples due to the random orientation with respect to the applied field and the strong critical field anisotropy. One issue which remains to be investigated is the effect on the nuclear relaxation rate of the flux line lattice and flux line fluctuations in the superconducting phase which was detected qualitatively in the enhancement of T_1T below T_c (see the inset of Fig. 3) but which would require aligned powder samples or single crystals to be investigated quantitatively.

[1] J. Nagamatsu, N. Nakagawa, T. Muranaka, Y. Zenitani, and J. Akimitsu, Nature (London) **410**, 63 (2001).

[2] S.L. Bud'ko, G. Lapertot, C. Petrovic, C.E. Cunningham, N. Anderson, and P.C. Canfield, Phys. Rev. Lett. **86**, 1877 (2001).

[3] D.G. Hinks, H. Claus, and J.D. Jorgensen, Nature (London) **411**, 457 (2001).

[4] A. Rigamonti, F. Borsa, and P. Carretta, Rep. Prog. Phys. **61**, 1367 (1998).

[5] J.K. Jung, S.H. Baek, F. Borsa, S.L. Bud'ko, G. Lapertot, and P.C. Canfield, Phys. Rev. B **64**, 012514 (2001).

[6] A.V. Tsvyashchenko *et al.*, Solid State Commun. **119**, 153 (2001).

[7] M. Mali, J. Roos, A. Shengelaya, H. Keller, and K. Conder, Phys. Rev. B **65**, 100518(R) (2002).

[8] G. Papavassiliou, M. Pissas, M. Fardis, M. Karayanni, and C. Christides, Phys. Rev. B **65**, 012510 (2001).

[9] H. Kotegawa, K. Ishida, Y. Kitaoka, T. Muranaka, and J. Akimitsu, Phys. Rev. Lett. **87**, 127001 (2001).

[10] A. Gerashenko, K. Mikalhev, S. Verkhovskij, T. D'yachova, A. Tyutyunnik, and V. Zubkov, cond-mat/0102421 (unpublished).

[11] H. Tou, H. Ikejiri, Y. Maniwa, T. Ito, T. Takenobu, K. Prassides, and Y. Iwasa, cond-mat/0103484 (unpublished).

[12] D.K. Finnemore, J.E. Ostenson, S.L. Bud'ko, G. Lapertot, and P.C. Canfield, Phys. Rev. Lett. **86**, 2420 (2001).

[13] P.C. Canfield, D.K. Finnemore, S.L. Bud'ko, J.E. Ostenson, G. Lapertot, C.E. Cunningham, and C. Petrovic, Phys. Rev. Lett. **86**, 2423 (2001).

[14] A. Abragam, *Principles of Nuclear Magnetism* (Academic Press, London, 1961).

[15] F. Borsa and A. Rigamonti, J. Magn. Reson. **20**, 232 (1975).

[16] G.E. Pake, J. Chem. Phys. **16**, 327 (1948).

[17] D.R. Torgeson, R.G. Barnes, and R.B. Creel, J. Chem. Phys. **56**, 4178 (1972).

[18] E. Fukushima and S. B. W. Roeder, *Experimental Pulse NMR* (Addison-Wesley, New York, 1981).

[19] T.P. Onak, H. Landesman, R.E. Williams, and I. Shapiro, J. Phys. Chem. **63**, 1533 (1959).

[20] E.R. Andrew and D.P. Tunstall, Proc. Phys. Soc. London **78**, 1 (1961).

[21] E. Pavarini and I.I. Mazin, Phys. Rev. B **64**, 140504(R) (2001).

[22] K.D. Belashchenko, V.P. Antropov, and S.N. Rashkeev, Phys. Rev. B **64**, 132506 (2001).

[23] O.K. Andersen, Z. Pawlowska, and O. Jepsen, Phys. Rev. B **34**, R5253 (1986).

[24] Our results and those reported in Ref. 22 are in good agreement, except for the value of the contact contribution to the ^{11}B relaxation rate. For AlB$_2$ (MgB$_2$), the value reported in Ref. 22 is a factor 2 (a factor 4) larger than the one reported in the present work (in Ref. 21). There are two reasons that could cause this discrepancy. First, all the integrals involving $\dot{\phi}_l$ terms—which come from writing the matrix elements of the hyperfine field operators in the LMTO's basis—seem to have been neglected in Ref. 22. Second, in Ref. 22 a rather large B sphere radius was chosen. This choice might have produced some distortion of the electronic structure, and in particular a larger B s-projected DOS in both AlB$_2$ and MgB$_2$—as one may see, e.g., comparing Table I of Ref. 22 with the values reported in the present work and in Ref. 21.

[25] L.C. Hebel and C.P. Slichter, Phys. Rev. **113**, 1504 (1959).

[26] L.C. Hebel, Phys. Rev. **116**, 79 (1959).

[27] S.L. Bud'ko, V.G. Kogan, and P.C. Canfield, Phys. Rev. B **64**, 180506(R) (2001).

[28] F. Simon *et al.*, Phys. Rev. Lett. **87**, 047002 (2001).

[29] S. Lee, H. Mori, T. Masui, Y. Eltsev, A. Yamamoto, and S. Tajima, J. Phys. Soc. Jpn. **70**, 2255 (2001).

[30] Y. Kitaoka (private communication).

[31] As a proof of the existence of two superconducting gaps in MgB$_2$, see for example F. Giubileo *et al.*, Phys. Rev. Lett. **87**, 177008 (2001), and references therein.